

# Polymorphism of syndiotactic polystyrene crystals from multiscale simulations

Chan Liu,<sup>1</sup> Kurt Kremer,<sup>1</sup> and Tristan Berau<sup>1, a)</sup>

Max Planck Institute for Polymer Research, Ackermannweg 10, 55128 Mainz, Germany

(Dated: 4 May 2019)

Syndiotactic polystyrene (sPS) exhibits complex polymorphic behavior upon crystallization. Computational modeling of polymer crystallization has remained a challenging task because the relevant processes are slow on the molecular time scale. We report herein a detailed characterization of sPS-crystal polymorphism by means of coarse-grained (CG) and atomistic (AA) modeling. The CG model, parametrized in the melt, shows remarkable transferability properties in the crystalline phase. Not only is the transition temperature in good agreement with atomistic simulations, it stabilizes the main  $\alpha$  and  $\beta$  polymorphs, observed experimentally. We compare in detail the propensity of polymorphs at the CG and AA level and discuss finite-size as well as box-geometry effects. All in all, we demonstrate the appeal of CG modeling to efficiently characterize polymer-crystal polymorphism at large scale.

## I. INTRODUCTION

The crystallization of molecular assemblies often involves the stabilization of a variety of distinct conformers, denoted polymorphism.<sup>1</sup> The impact of polymorphs, may it be thermodynamic, structural, or physiological, makes their understanding and prediction essential for a broad area of research, from hard condensed matter to organic materials. The computational modeling of crystalline materials has rapidly developed in recent years, from crystallization<sup>2,3</sup> to predicting polymorphs and their relative stability<sup>4-7</sup>. These developments are remarkable given the complexity of the system: from the molecular architecture to sampling challenges at low temperatures to the significant timescales involved. For this reason, past computational studies focused on crystallization and/or polymorphism have been limited to molecular crystals—based on small molecules. Here instead, we extend the computational characterization of polymers crystals,<sup>8-11</sup> by modeling for the first time its self assembly and resulting polymorphs.

Syndiotactic polystyrene (sPS) is known for its unusual crystal polymorphism. Five different crystalline forms have been reported experimentally. Fig. 1 shows three main forms studied in this work. The unit cells are projected onto the  $a - b$  plane, and the backbones of the chains are along the  $c$  axis. Experimentally, two types of crystalline phases have been identified: the zig-zag-chain forming  $\alpha$ <sup>12-15</sup> and  $\beta$ <sup>16,17</sup> appear upon thermal annealing of a melt, whereas the other three helix-forming crystalline phases,  $\gamma$ <sup>18,19</sup>,  $\delta$ <sup>20-22</sup> and  $\varepsilon$ <sup>23-25</sup> are obtained by solution processing. The  $\alpha$  and  $\beta$  forms of sPS are further classified into the limiting disordered forms ( $\alpha'$  and  $\beta'$ ) and limiting ordered forms ( $\alpha''$  and  $\beta''$ )<sup>12,14,16,26</sup>. In particular, melt crystallization procedures generally produce the limiting ordered  $\alpha''$  and limiting disordered  $\beta'$  models<sup>26</sup>. The limiting disordered  $\alpha'$  model is obtained by annealing the amorphous sample<sup>26</sup>, whereas

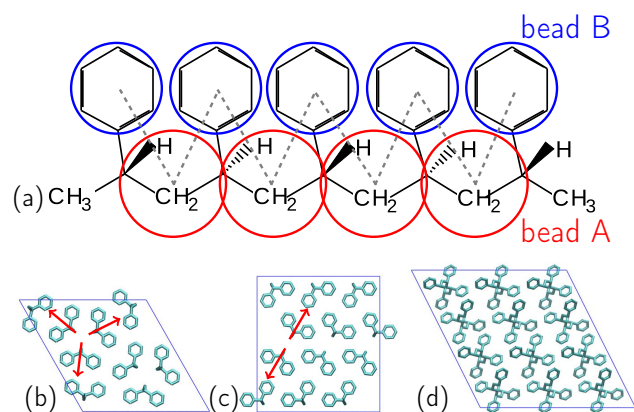


FIG. 1. (a) Representation of syndiotactic polystyrene, including the CG mapping scheme: each monomer is mapped onto two coarse-grained beads. CG bead A is the center of mass of the backbone connecting two sidechains, while bead B is the center of mass of the phenyl group. Polymorphism: (b)  $\alpha$ , (c)  $\beta$ , (d)  $\delta$  forms.

the limiting ordered  $\beta''$  model is obtained by crystallization from solution, when the solvent is rapidly removed at higher temperatures above  $150^\circ\text{C}$ <sup>16</sup>. Two of the helical crystalline phases ( $\delta$  and  $\varepsilon$ ) can only be obtained by guest removal from co-crystalline phases. The  $\delta_e$  form is transformed into the solvent-free  $\gamma$  form by annealing above  $130^\circ\text{C}$ <sup>18,20,26</sup>. These findings illustrate that the experimentally-observed structures depend on the experimental processing, making conclusions about their thermodynamic equilibrium difficult.

Several molecular simulation studies have been performed to better understand the nanoporous cavity structures formed by crystalline syndiotactic polystyrene. Tamai and his co-workers<sup>27</sup> studied the size, shape and connectivity of the cavities in the crystal  $\alpha$ ,  $\beta$  and  $\delta$  forms. Some other properties were also studied, such as diffusion of gases<sup>28,29</sup>, reorientational motion of guest solvents<sup>30,31</sup>, and sorption of small molecules<sup>32-34</sup>. While these studies helped understand the behavior of specific

<sup>a)</sup>Electronic mail: berau@mpip-mainz.mpg.de

forms of sPS crystals, they did not address the crystallization process or the relative stability of the polymorphs. By studying sPS on the nanosecond timescale, they could not observe self assembly and spontaneous polymorph interconversion, due to their metastability. Yamamoto observed the onset of isotactic polypropylene crystallization, but leading to a smectic mesophase instead of crystal polymorphs<sup>35</sup>. The simulation of polymer crystallization remains challenging because these processes are slow on the molecular time scale. In addition, the simulated chain lengths must be large enough to link to experimentally realistic situations<sup>36</sup>. As an alternative to atomistic (AA) simulations, coarse-grained (CG) models<sup>37–39</sup> combine a number of atoms into superatoms or beads to significantly speed up the simulations, while potentially retaining enough chemical detail to differentiate polymorphs. Its capability to reach longer length and timescales is strengthened by an observation we present below: the relatively small systems we can afford at the AA level display finite-size effects.

Several CG models for polystyrene have been reported, but so far focusing solely on the amorphous phase. In several models one CG bead represents a single monomer<sup>40–43</sup>. Milano and Mueller-Plathe<sup>40,41</sup> center the beads on methylene carbons. The model of Qian and coworkers<sup>42</sup> places the bead on the center of mass of the monomer. Both of these models use different bead types to represent different types of diads, thus keeping information about the chain stereosequences. Sun and Faller<sup>43</sup> center the beads on the backbone carbons to which the phenyl rings are attached. In this model, each bead represents one PS monomer without distinguishing between different types of diads. Single-bead representations for a polystyrene monomer represent significant issues to describe polymorphism, as they lack the necessary degrees of freedom to distinguish between the relevant forms. Models of higher resolution were also developed: Harmandaris and coworkers<sup>44,45</sup> devised two different two-bead-per-monomer models. In their first model<sup>44</sup>, the CH<sub>2</sub> group of the backbone chain is represented by one CG bead, whereas the remaining CH group of the monomer in the backbone and its pendant phenyl ring are represented by another CG bead. In their second model<sup>45</sup>, the phenyl ring is represented by one CG bead, while the other bead represents the CH<sub>2</sub> of the backbone as well as a contribution from each one of the two neighboring CH groups. By comparison, the second mapping scheme better reproduces the local chain conformations and melt packing observed in atomistic simulations. Based on this mapping scheme, Fritz and coworkers<sup>46</sup> developed a new CG force field using the conditional reversible work (CRW) method<sup>47,48</sup>, a thermodynamic-based CG method that samples isolated atomistic chains or pairs of oligomers in vacuum. In this paper, we find that this CG model can successfully crystallize sPS. The bonded force field seems to adequately reproduce the local chain conformations of syndiotactic polystyrene so that the sterics allow for crystallization.

More importantly, this finding illustrates the remarkable transferability properties of the CRW method.

In this paper, we report both AA and CG simulations of the temperature-driven phase transition between crystal and melt. Annealing simulations led to highly-ordered conformations, but exhibiting significant hysteretic behavior. Replica-exchange molecular dynamics (REMD) simulations helped the conformational sampling and the identification of the transition temperature. Backmapping of CG snapshots provided starting AA configurations. For both resolutions, we consider several polymorphs,  $\alpha$ ,  $\beta$  and  $\delta$ , observed experimentally. We find that the two models stabilize  $\alpha$  and  $\beta$ , but not  $\delta$ . We discuss the impact of finite-size effects and box geometries. To alleviate these artefacts, we use the CG model to construct a larger system and discuss the convergence of polymorph populations.

## II. METHODS

### A. Model

#### 1. AA Model

We used the atomistic (AA) model of polystyrene from Mueller-Plathe<sup>49</sup>. In this model, the phenyl groups are described using parameters from benzene, while the parameters for the aliphatic carbons and hydrogens were identical to aliphatic polymers. The rotation of the phenyl rings is left free. All bond lengths were constrained by the LINCS method<sup>50</sup>.

#### 2. CG Model

The CG polystyrene force field of Fritz *et al.*<sup>46</sup> is derived from the above-mentioned AA model. It maps each monomer onto two CG beads of different types, denoted A for the chain backbone and B for the phenyl ring (see Fig. 1a). We stress that the CG model represents PS by a *linear* chain, where the beads are connected by CG bonds A–B. There are no bonds between the A beads, and the close connection between them is reproduced indirectly by the angular potentials  $\theta_{ABA}$ . The tacticity of polystyrene is encoded in the potential parameters. Here we only use the parameters of syndiotactic polystyrene whose chains only consist of racemic diads.

The CG force field includes the bonded and nonbonded interaction potentials in a tabulated form and are derived separately. Potentials for bonded degrees of freedom of the CG model are obtained by direct Boltzmann inversion of distributions obtained from atomistic simulations of single chains in vacuum using stochastic dynamics.

The nonbonded potentials are derived by the conditional reversible work (CRW) method<sup>47,48</sup>. They are obtained from constraint dynamics runs with the all-atom model of two trimers (or fourmers) in vacuum. In these

runs the atoms mapping to a pair of beads A or B were held at fixed distance  $r$ . The pair potential of mean force (PMF),  $V_{\text{PMF}}$ , was calculated by

$$V_{\text{PMF}}(r) = \int_{r_m}^r ds [\langle f_c \rangle_s] + 2k_B T \ln r, \quad (1)$$

where  $k_B$  is the Boltzmann constant,  $T$  is the temperature,  $f_c$  is the constraint force between the two CG mapping points,  $\langle \cdot \rangle_s$  is a constrained ensemble average, and  $r_m$  is the maximum distance between the two mapping points.

The effective, nonbonded A–A interaction potential is next obtained from

$$V_{\text{eff}}^{\text{AA}}(r) = V_{\text{PMF}}^{\text{AA}}(r) - V_{\text{PMF}}^{\text{excl,AA}}(r) \quad (2)$$

where the second PMF,  $V_{\text{PMF}}^{\text{excl,AA}}$ , is along the same coordinate  $r$  but excludes all direct A–A atomistic interactions while maintaining all other interactions with and between neighboring parts of the oligomers. A similar procedure is applied to A–B and B–B.

One advantage of this approach is that it is computationally inexpensive. More importantly, this approach is widely different from many other CG methods that use information on condensed-phase properties of the melt state as input in the development of the effective potentials. This crucial difference enables the greater transferability reported herein.

## B. Replica exchange simulations

Replica exchange molecular dynamics (REMD)<sup>51</sup> is used to enhance the sampling of computer simulations, especially when metastable states are separated by relatively high energy barriers. It involves simulating multiple replicas of the same system at different temperatures and randomly exchanging the complete state of two replicas at regular intervals with a Metropolis criterion.

All simulations reported in this study were performed using the molecular dynamics package GROMACS 4.6<sup>52</sup>. The integration time step of the AA model was 1 fs. AA-RE simulations were performed with 48 (56 for the  $\beta$  form) temperatures from 250 K to 550 K (700 K for the  $\beta$  form), and replica exchange was attempted every 1 ps. Simulations were carried out in the  $NPT$  ensemble using the stochastic velocity rescaling thermostat<sup>53</sup> ( $\tau_T^{\text{AA}} = 0.2$  ps) and the Berendsen barostat<sup>54</sup> ( $\tau_P^{\text{AA}} = 2$  ps). For the CG model, the integration time step was  $10^{-3} \tau$ , where  $\tau$  defines the reduced unit of time in the CG model. CG-RE simulations were performed with 48 temperatures from 250 K to 550 K, and replica exchange was attempted every  $\tau$ . In CG simulations, we also employed the stochastic velocity rescaling thermostat ( $\tau_T^{\text{CG}} = 0.2 \tau$ ) and the Berendsen barostat ( $\tau_P^{\text{CG}} = 2 \tau$ ). Note that in all replica exchange simulations, we use isotropic pressure coupling, which means that the angles of the simulation box are

fixed. We have found that anisotropic coupling led to large fluctuations close to the phase transition.

## C. Order parameter

Orientalional order parameters are useful indicators of crystal formation and crystal growth. In this work, calculating order parameters in both AA and CG simulations is based on geometries at the CG level, and we take one racemic diad (two monomers) as one characterizing unit. In a polymer chain, for a side-chain bead  $B_1^i$  in unit  $i$  (see Fig. 2), we identify an orientation vector which points from  $B_1^i$  to  $B_1^{i+1}$  and normalize it to a unit vector

$$\mathbf{e}_i = \frac{\mathbf{r}_{i+1} - \mathbf{r}_i}{|\mathbf{r}_{i+1} - \mathbf{r}_i|}. \quad (3)$$

Similar orientation vectors can be obtained for bead  $A_1^i$ ,  $A_2^i$  and  $B_2^i$ . For two given orientation vectors  $\mathbf{e}_i$  and  $\mathbf{e}_j$ , the order parameter between them is calculated as follows<sup>55</sup>:

$$P_{ij} = \frac{3}{2}(\mathbf{e}_i \cdot \mathbf{e}_j)^2 - \frac{1}{2}. \quad (4)$$

The order parameter of the whole system is the average over all possible  $P_{ij}$  in the system.

Note that this order parameter has some limitations: it can only recognize trans-planar chain conformations. As mentioned in the introduction, syndiotactic polystyrene has five different crystalline forms. To further study the phase transition between these different forms, we developed a procedure to characterize the different forms in these ordered states.

## D. Form characterization

In analogy to the order parameter, form characterization in both AA and CG simulations is based on conformations at the CG level, and we take two monomers as one characterizing unit.

There are two types of single-chain conformations (see Fig. 2): trans-planar chains ( $\alpha$  and  $\beta$ ) and helical chains ( $\gamma$ ,  $\delta$  and  $\varepsilon$ ). First, we identify these two different crystalline chain conformations from amorphous chains. In a polymer chain, for unit  $i$ , we identify a backbone vector  $\mathbf{b}_i$  which points from bead  $A_2^i$  to bead  $A_1^i$ . When the angle between vector  $\mathbf{b}_i$  and vector  $\mathbf{b}_{i+1}$  is around  $0^\circ$ , the unit  $i$  and  $i+1$  are trans-planar chain segments (see Fig. 2 (a)). When the angle between vector  $\mathbf{b}_i$  and vector  $\mathbf{b}_{i+1}$  is around  $70^\circ$  and the angle between vector  $\mathbf{b}'_i$  (from bead  $A_1^{i+1}$  to bead  $A_2^i$ ) and vector  $\mathbf{b}_i$  is around  $25^\circ$ , the unit  $i$  and  $i+1$  are helical chain segments (see Fig. 2 (b)). The remaining segments are considered amorphous.

For trans-planar chain segments, we discriminate crystal regions between different chain-stretching directions.

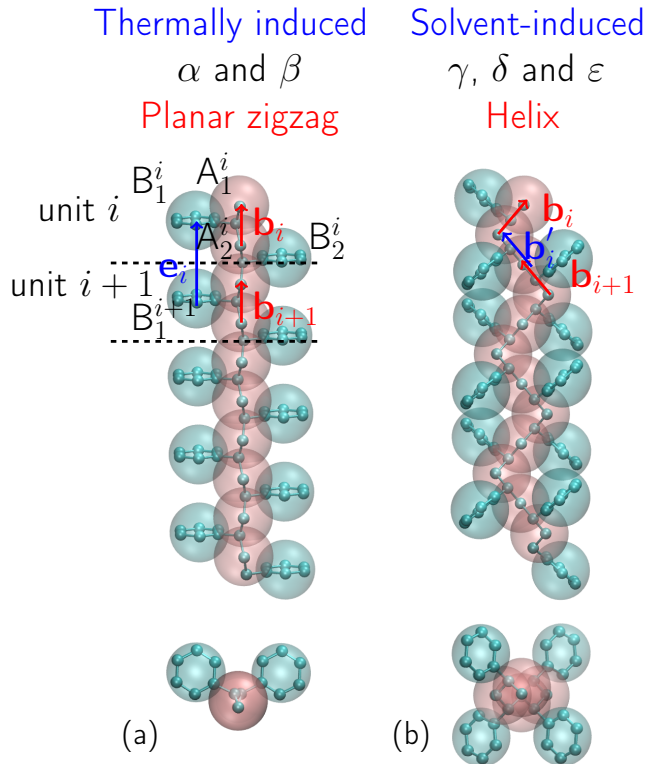


FIG. 2. Five different crystalline forms: two crystalline phases ( $\alpha$  and  $\beta$ ) with trans-planar chains; three crystalline phases ( $\gamma$ ,  $\delta$  and  $\varepsilon$ ) with the  $s(2/1)2$  helical chains.

Then in each region and each single layer, which is perpendicular to the chain stretching direction, we measure the distances between all beads of type A in the same layer. When the distances between two such beads is smaller than 0.6 nm, we associate them into the same group. In each group, we measure the orientations of side chains to identify  $\alpha$  and  $\beta$  forms (see Fig. 1(b)(c)). If the orientations are all parallel, the group is a “full  $\beta$ ” group; if the angles of the orientations are all around  $120^\circ$ , the group is a “full  $\alpha$ ” group. Some groups have features of both  $\alpha$  and  $\beta$  forms, in which case we call them “mix” (see Fig. 7). In case only a single characterizing unit is found in the group, we call it “defect.”

In this work, we focus on the main  $\alpha$  and  $\beta$  polymorphs found in annealing experiments, while all helical chain segments are herein called  $\delta$  for convenience.

### III. RESULTS AND DISCUSSION

#### A. Crystallization of the CG model

##### 1. CG annealing simulations

Since the CG model of Fritz *et al.*<sup>46</sup> derived using CRW method from AA simulations can predict melt properties,

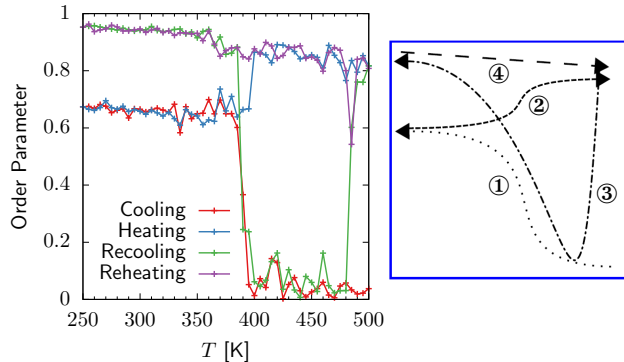


FIG. 3. Evolution of a representative structural order parameter (where a value of 1 is completely ordered and 0 is disordered) during the cooling, heating, recooling and reheating CG-MD simulations.

including the melt packing and the density between 400 and 520 K, we use this model to perform annealing simulations to test its ability to crystallize. The initial system is an sPS melt that contains 9 chains, each comprising 10 monomers. To crystallize the system, annealing simulation is performed from  $T = 500$  K to  $T = 250$  K, with a total cooling time of  $2.5 \times 10^5 \tau$ . This is then followed by a heating procedure back to  $T = 500$  K at the same rate. The evolution of a commonly-used structural order parameter during the cooling, heating, recooling and reheating processes is displayed in Fig. 3. Note that the simulation box is rectangular under isotropic pressure coupling. It shows that highly-ordered conformations can indeed be obtained from annealing simulations, but the fast annealing rate leads to significant hysteresis.

#### 2. Replica exchange simulations from CG and AA models

To improve the sampling efficiency and accurately characterize the transition behavior, we employed replica exchange molecular dynamics (REMD)<sup>51</sup> in the CG and AA simulations. Simulating a crystallization process using an atomistic model is difficult. Backmapping is a good strategy to reconstruct an atomistic configuration from a CG snapshot. We use backmapping to generate a highly ordered atomistic configuration, which is taken as the initial structure in the AA simulations. Fig. 4(a) shows that both AA and CG replica exchange simulations display a phase transition, and the transition temperatures are both around 450 K. This indicates that this CG model can reproduce the phase transition of sPS roughly at the correct temperature. This overall hints at remarkable transferability of the CG model between the melt and the crystal.

However, some differences appear between these two models at low temperatures. Fig. 4 (b) and (c) show multiple peaks in the order-parameter distributions of the AA model, while only two peaks are found in the

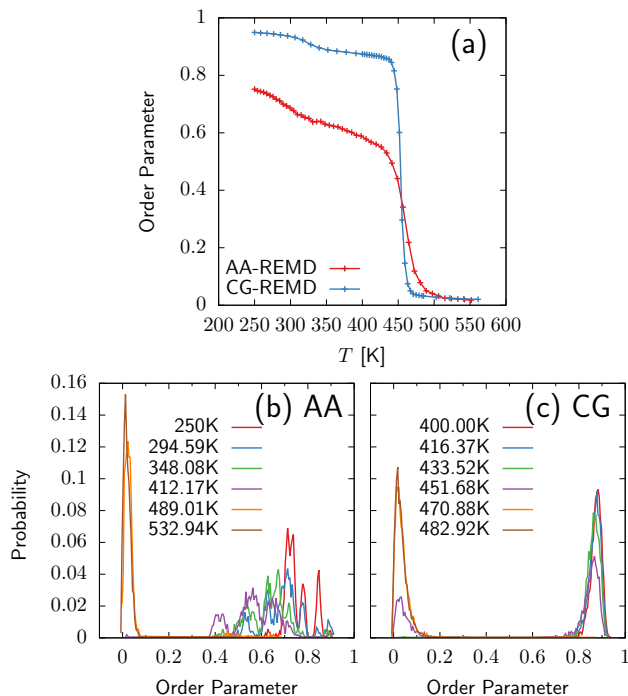


FIG. 4. (a) Structural order parameter as a function of temperature obtained from AA and CG REMD simulations. Structural order-parameter distributions as a function of temperature: (b) AA and (c) CG.

CG model. The CG model fails to display the structural heterogeneity of its AA counterpart.

## B. Crystal polymorphs

To further explore crystallization of sPS, we consider the different crystal forms observed experimentally. The crystalline polymorphs studied in this paper are listed in Tab. I. We perform atomistic and coarse-grained replica exchange simulations from these different crystal structures. Fig. 5 shows that three different initial configurations lead to different thermodynamics because of size effects and box shapes. In the following we analyze the results in detail.

### 1. $\alpha$ form

Fig. 5 (a) shows the initial  $\alpha$  form configuration, which contains 9 chains of 10 monomers each. RE simulations were performed for both the CG and AA models for  $1.2 \times 10^6 \tau$  and 300 ns, respectively. Fig. 5 (a-1) and (a-2) shows the polymorph distributions in the temperature range 250 – 550 K. At both resolutions in this box geometry, the  $\alpha$  form is not only stable but also predominant, with a transition temperature around 460 K.

Fig. 6 (a) shows the initial CG configuration, set up in

an  $\alpha''$  form, as determined by X-ray diffraction experiments<sup>14</sup>. The limiting-ordered  $\alpha''$  form is characterized by a specific positioning of triplets of chains, e.g., one triplet is oriented in one direction, while the other two in the opposite directions. The limiting disordered  $\alpha'$  form, on the other hand, has a statistical disorder between these two orientations of triplets of chains. Fig. 6 (b) shows a representative snapshot obtained from CG-RE simulations at 250 K. We find that all the triplets of chains sampled from the CG model always display the same arrangement of triplets—characteristic of  $\alpha'$ —while  $\alpha''$  does not seem stable in the CG model.

### 2. $\beta$ form

Fig. 5 (b) shows the initial  $\beta$  configuration, containing 12 chains of 10 monomers each. We performed RE simulations for the CG and AA models for  $2 \times 10^6 \tau$  and 200 ns, respectively. The CG model predominantly stabilizes a mixture of  $\alpha$  and  $\beta$  forms below the transition temperature (see Fig. 5 (b-1)). While many snapshots are made of large homogeneous regions of  $\alpha$  or  $\beta$  polymorphs, we also find a significant population that mix the two, denoted “mix” (Fig. 7). The presence of  $\alpha/\beta$  mixtures breaks the long-range order expected in homogeneous phases and resembles a form of intermediate between the two polymorphs. This mixing has not been reported experimentally.

Fig. 8(a) shows the order parameter as a function of temperature obtained from CG and AA REMD simulations. Comparing the two resolutions, we find that the transition temperatures agree when simulated in the  $\alpha$ -compatible box shape, but not for  $\beta$ . The AA model shows a much more stable  $\beta$  form than the other scenarios: a transition temperature around 600 K, compared to 430–450 K otherwise. In the CG simulations, the transition temperature of the  $\beta$  form is around 430 K, roughly 20 K lower than the  $\alpha$  form. Experimentally, crystallization of a melt leads preferentially to the  $\alpha$  ( $\beta$ ) crystals when cooled from low (high) temperatures<sup>56</sup>. The AA model is thus in qualitative agreement with the preferential behavior for  $\beta$  found experimentally.

To further study the  $\beta$  form in CG simulations, we compare  $\beta$  configurations that are representative of our CG-RE simulations with the  $\beta''$  form observed experimentally<sup>17</sup>. Fig. 8 (b) shows there are two kinds of bilayers, indicated as A(/) and B(\). The two bilayers are characterized by different orientations of the lines connecting two adjacent phenyl rings inside each chain. The regular succession of bilayers ABAB gives rise to the ordered  $\beta''$  form, also showing that these two orientations are not parallel to the layer lines. On the other hand, CG configurations have bilayers parallel to the layer lines (Fig. 8 (c)).

The densities obtained from AA and CG simulations are listed in Tab. II, compared with experimental data. While the temperature dependence shown in Fig. 8 (a)

TABLE I. Main crystal structures of s-PS studied in this work, along with the number of crystal units, number of chains and number of monomers for each chain in the MD simulation.

Crystal	a (Å)	b (Å)	c (Å)	$\gamma$ (°)	Space group	Conformation	$N_{unit}$	$N_{chain} \times N_{mon}$
$\alpha^{14}$	25.82	26.26	5.03	119.9	$P3$	$TTTT$	$1 \times 1 \times 5$	$9 \times 10$
$\beta^{17}$	8.79	28.61	5.04	90.0	$P2_12_12_1$	$TTTT$	$3 \times 1 \times 5$	$12 \times 10$
$\delta^{20}$	17.38	11.73	7.81	115.0	$P2_1/a$	$(TTGG)_2$	$3 \times 2 \times 3$	$12 \times 12$

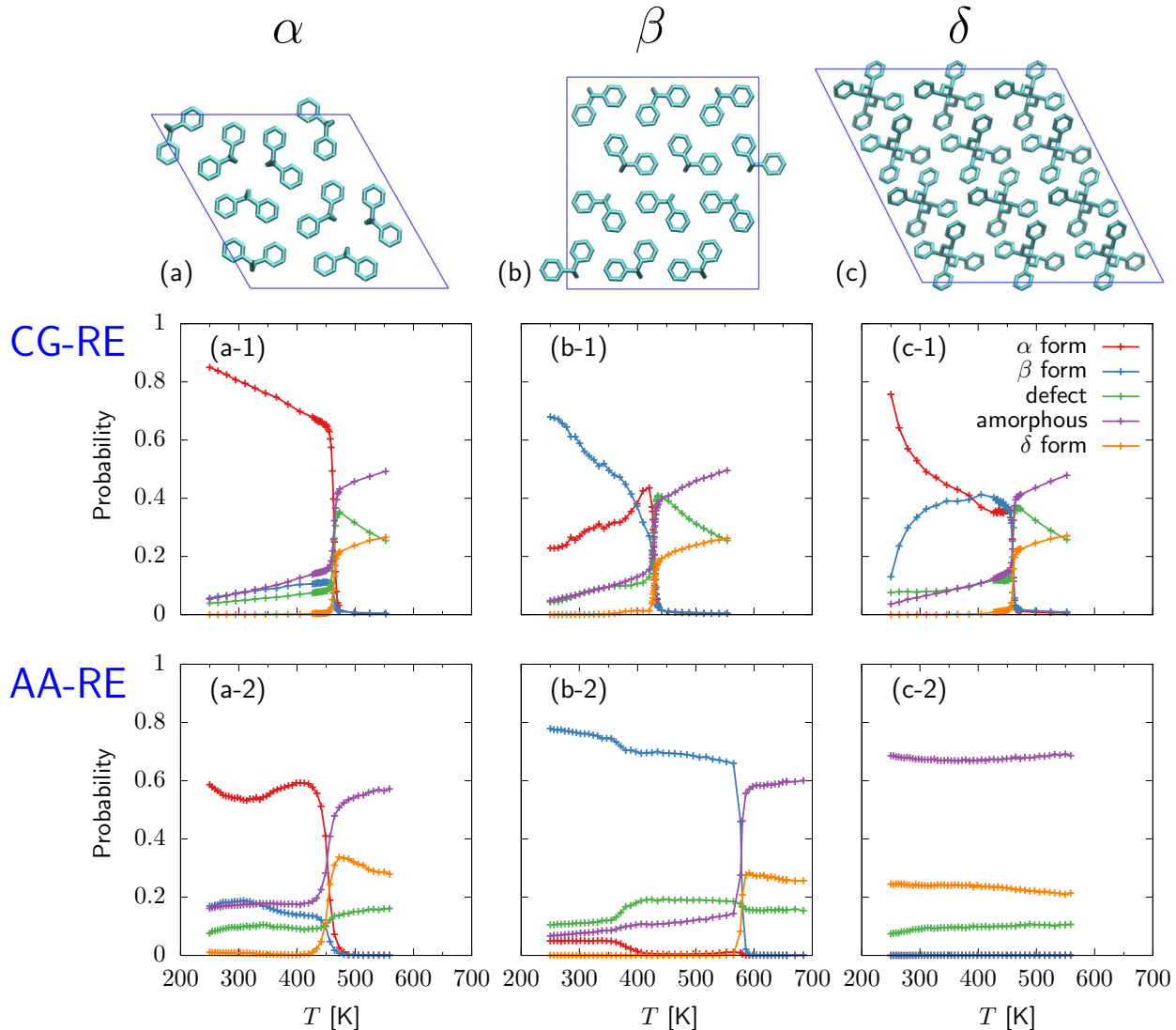


FIG. 5. From top to bottom: Initial crystal structures for (a)  $\alpha$ , (b)  $\beta$  and (c)  $\delta$  polymorphs; distributions of polymorphs as a function of temperature obtained from CG and AA REMD simulations.

resulted from the average effect of different phases, here we discriminate between them. The results show that the AA simulations reproduce the experimental values satisfactorily. The CG results are somewhat larger: While the  $\alpha$  form in CG simulations remains in reasonable agreement with both references, the  $\beta$  form is markedly higher.

These results hint at structural deficiencies for the  $\beta$  form in the CG model, both in terms of limited packing orientations (8) and higher density. We hint at the

limited modeling of  $\pi$ -stacking interactions between side chains, as well as the packing of phenyl hydrogens (e.g., T-like stacking). This structural deficiency, leading to reduced stabilization of the  $\beta$  form, may well explain the transition-temperature offset.

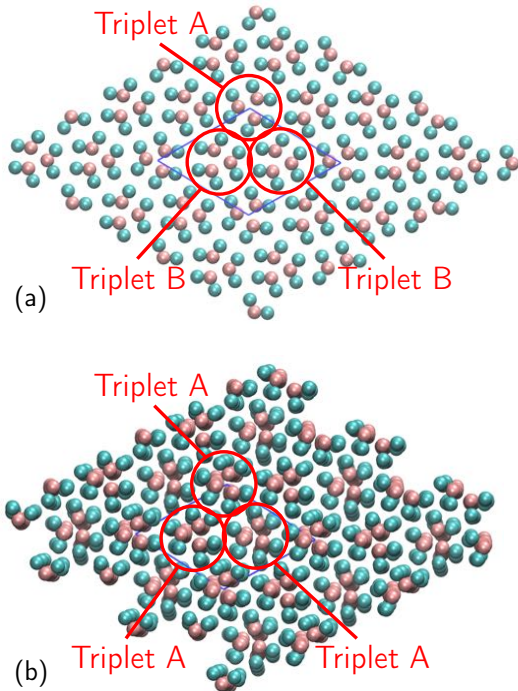


FIG. 6. (a) The initial  $\alpha''$  configuration. (b) A representative CG-RE snapshot sampled at 250 K, belonging to the  $\alpha'$  form.

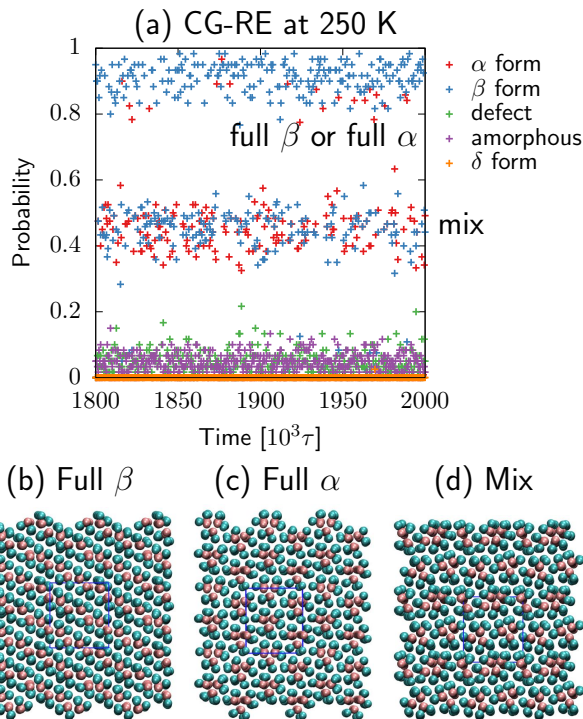


FIG. 7. (a) Distributions of polymorphs in the last  $2 \times 10^5 \tau$  of the CG-RE simulations at 250 K. (b) Full  $\beta$ , (c) full  $\alpha$ , (d) and mixture at 250K.

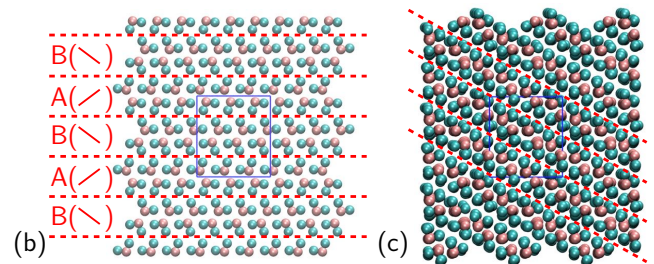
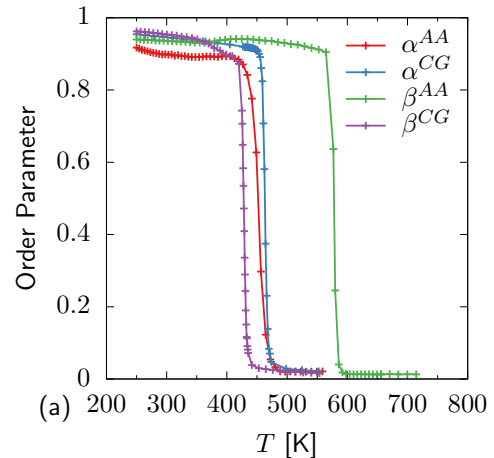


FIG. 8. (a) Structural order parameter as a function of temperature obtained from CG and AA REMD simulations. (b) The initial  $\beta''$  configuration. (c) Representative snapshot obtained from CG-RE simulations at 250 K.

TABLE II. Density of s-PS polymorphs ( $\text{g}/\text{cm}^3$ ).

Crystal	experiment	AA simulation	CG simulation
$\alpha$	1.034	1.075	1.098
$\beta$	1.08	1.078	1.208
$\delta$	0.977	-	-

### 3. $\delta$ form

Fig. 5(c) shows the initial  $\delta$  form configuration, containing 12 chains with 12 monomers each. RE simulations at the CG and AA level were performed for  $1.6 \times 10^6 \tau$  and 100 ns, respectively. Fig. 5 (c-1) shows that the  $\delta$  form is not stable at low temperatures at the CG level— $\alpha$  and  $\beta$  form coexist instead. This phenomenon is consistent with experimental studies, since we are not modeling the cosolvent necessary to stabilize the  $\delta$  form. At 250 K, the system favors the  $\alpha$  form over  $\beta$ , possibly because the geometry of the unit cell is more congruent with the former.

At the AA level, we observed no crystallization (Fig. 5 (c-2)). While we do expect the system to eventually crystallize, we suppose that our simulation times—even using RE—did not allow to probe long-enough timescales to reach any reasonable equilibrium. While AA simulations in the  $\alpha$  and  $\beta$  geometries did stabilize crystals, we observed little dynamical exchange among them, further

suggesting the sampling challenge of polymer crystals at an AA resolution.

#### 4. Melt structure

At high temperatures the system consists of amorphous, defects, and a minor population of  $\delta$ -type configurations. Note that  $\delta$ -type phases here refer to the presence of helical chain segments, while defect correspond to chain segments that are planar but falling out of the  $\alpha$  and  $\beta$  forms. A comparison of the melt populations between the two resolutions shows the larger occurrence of planar conformations (i.e., defect) at the CG level. On the other hand, amorphous and helical conformations have a somewhat higher population at the AA level. This indicates that the CG model of sPS tends to favor planar arrangements. Here again, the packing of the phenyl rings may play a role, in accordance with the high density found for  $\beta$ .

#### C. Toward larger systems

In the previous sections, we demonstrated that the thermodynamic-based CG model applied here can crystallize and stabilize major polymorphs. Given the sampling difficulties already met at the AA level, we consider larger systems only with the CG model: 96 chains of 10 monomers each. The CG-RE simulations ran for  $7 \times 10^5 \tau$ .

Fig. 9 (a) shows one snapshot starting from the  $\beta$  form, where  $\alpha$ ,  $\beta$  and the mixed phases exist simultaneously in the crystalline state. Full  $\alpha$  or  $\beta$  forms, observed in the small systems, are not found here. At low temperatures, the proportion of  $\alpha$  is a bit higher than  $\beta$  (Fig. 9 (b)). It is worth mentioning that we also performed another simulation starting from the  $\alpha$  form (72 chains), and obtained virtually the same proportion of  $\alpha$  and  $\beta$  forms. These converging results thus indicate that they do not depend on the chosen box geometry, unlike the abovementioned findings on the smaller systems. Unfortunately, this result is not consistent with experiments, which associates a higher stability to the  $\beta$  form. This stands as another evidence of the structural deficiency of the  $\beta$  form in this CG model.

Fig. 9(c) shows that, compared with the small system, the transition temperature of the large system is a bit lower: 400 K. Fig. 9(d) shows the order-parameter distributions at different temperatures, which show more structural heterogeneity than found earlier on (Fig. 4 (c)). We conclude that the larger system self-assembles more diverse crystalline phases that dynamically interconvert, leading to an overall reduction in the transition temperature compared to the small systems.

Interestingly, while the  $\alpha$  form was predominantly sampled when simulating a smaller box congruent with the  $\alpha$  unit cell (Fig. 5), this preferential stabilization was not

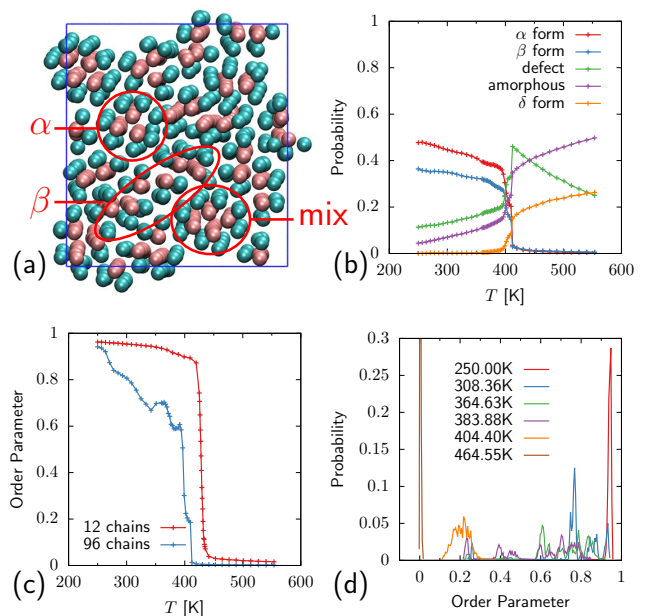


FIG. 9. CG simulations: (a) Representative snapshot made from 96 chains at 250K; (b) CG Distributions of polymorphs as a function of temperature; (c) Structural-order parameter as a function of temperature obtained (comparison between 12 chains and 96 chains); and (d) Structural order parameter distributions at different temperatures.

observed here for the larger system. Experimental results have suggested that formation of the  $\alpha$  form may be a kinetically-controlled process.<sup>26</sup> Our results, while devoid of non-equilibrium aspects, hint at a templating mechanism that favors the formation of  $\alpha$  due to the environment.

#### IV. CONCLUSION

We report the first computational studies of polymer-crystal polymorphism. Replica exchange molecular dynamics simulations are performed using atomistic (AA) and coarse-grained (CG) models to model the thermal crystallization of syndiotactic polystyrene (sPS). Remarkably, the thermodynamic-based CG model not only reproduces melt properties, but also transfers to the crystals. Furthermore, we find that the CG model stabilizes the main polymorphs  $\alpha$  and  $\beta$ , while the  $\delta$  form was not observed due to the lack of solvent. These results are in qualitative agreement with experiments. Our simulations suggest the role of templating mechanisms to rationalize the experimentally-observed kinetic control of the  $\alpha$  form. Because the CG model markedly speeds up the simulations, it can be used to simulate significantly larger systems, better suited to study crystallization without finite-size effects. We thus show that CG models are powerful tools to investigate the polymorphic behavior of polymers. The choices of mapping scheme

and force field are important to stabilize and distinguish the main polymorphs. In spite of remaining shortcomings, the ability of the CG model (without additional tuning) to reproduce the crystallization transition and polymorphism of polymer is remarkable. We expect CG simulations to become a major tool for polymer-crystal polymorphism studies.

## V. ACKNOWLEDGMENT

We thank Christine Peter, Omar Valsson, and Claudio Perego for critical discussions and reading of the manuscript. T.B. acknowledges funding from the Emmy Noether program of the Deutsche Forschungsgemeinschaft (DFG).

- <sup>1</sup>Bernstein J. Polymorphism in molecular crystals. Oxford University Press, 2002.
- <sup>2</sup>Perego C, Salvalaglio M, Parrinello M. Molecular dynamics simulations of solutions at constant chemical potential. *The Journal of Chemical Physics*, 2015, 142(14): 144113.
- <sup>3</sup>Radu M, Kremer K. Enhanced crystal growth in binary Lennard-Jones mixtures. *Physical Review Letters*, 2017, 118(5): 055702.
- <sup>4</sup>Beran G J O. Modeling polymorphic molecular crystals with electronic structure theory. *Chemical Reviews*, 2016, 116(9): 5567-5613.
- <sup>5</sup>Price S L. Predicting crystal structures of organic compounds. *Chemical Society Reviews*, 2014, 43(7): 2098-2111.
- <sup>6</sup>Marom N, DiStasio Jr. R A, Atalla V, et al. Many-Body dispersion interactions in molecular crystal polymorphism. *Angewandte Chemie*, 2013, 52: 6629-6632.
- <sup>7</sup>Reilly A M, Tkatchenko A. Role of dispersion interactions in the polymorphism and entropic stabilization of the Aspirin crystal. *Physical Review Letters*, 2014, 113(5): 055701.
- <sup>8</sup>Hu W, Frenkel D. Polymer crystallization driven by anisotropic interactions. *Interphases and Mesophases in Polymer Crystallization III*, 2005, 191: 1-35.
- <sup>9</sup>Sommer J U, Luo C. Molecular dynamics simulations of semicrystalline polymers: crystallization, melting, and reorganization. *Journal of Polymer Science Part B: Polymer Physics*, 2010, 48(21): 2222-2232.
- <sup>10</sup>Yamamoto T. Molecular dynamics of polymer crystallization revisited: Crystallization from the melt and the glass in longer polyethylene. *The Journal of Chemical Physics*, 2013, 139(5): 054903.
- <sup>11</sup>Welch P M. Examining the role of fluctuations in the early stages of homogenous polymer crystallization with simulation and statistical learning. *The Journal of Chemical Physics*, 2017, 146(4): 044901.
- <sup>12</sup>De Rosa C, Guerra G, Petraccone V, et al. Crystal structure of the  $\alpha$ -form of syndiotactic polystyrene. *Polymer Journal*, 1991, 23(12): 1435-1442.
- <sup>13</sup>Corradini P, De Rosa C, Guerra G, et al. Conformational and packing energy of the crystalline  $\alpha$  modification of syndiotactic polystyrene. *European Polymer Journal*, 1994, 30(10): 1173-1177.
- <sup>14</sup>De Rosa C. Crystal structure of the trigonal modification ( $\alpha$  form) of syndiotactic polystyrene. *Macromolecules*, 1996, 29(26): 8460-8465.
- <sup>15</sup>Cartier L, Okihara T, Lotz B. The  $\alpha''$  "superstructure" of syndiotactic polystyrene: A frustrated structure. *Macromolecules*, 1998, 31(10): 3303-3310.
- <sup>16</sup>De Rosa C, Rapacciuolo M, Guerra G, et al. On the crystal structure of the orthorhombic form of syndiotactic polystyrene. *Polymer*, 1992, 33(7): 1423-1428.
- <sup>17</sup>Chatani Y, Shimane Y, Ijitsu T, et al. Structure study on syndiotactic polystyrene: 3. Crystal structure of planar form I. *Polymer*, 1993, 34(8): 1625-1629.
- <sup>18</sup>Rizzo P, Lamberti M, Alburnia A R, et al. Crystalline orientation in syndiotactic polystyrene cast films. *Macromolecules*, 2002, 35(15): 5854-5860.
- <sup>19</sup>Rizzo P, Alburnia A R, Guerra G. Polymorphism of syndiotactic polystyrene:  $\gamma$  phase crystallization induced by bulky non-guest solvents. *Polymer*, 2005, 46: 9549-9554.
- <sup>20</sup>De Rosa C, Guerra G, Petraccone V, et al. Crystal structure of the emptied clathrate form ( $\delta_e$  form) of syndiotactic polystyrene. *Macromolecules*, 1997, 30(14): 4147-4152.
- <sup>21</sup>Milano G, Venditto V, Guerra G, et al. Shape and volume of cavities in thermoplastic molecular sieves based on syndiotactic polystyrene. *Chemistry of Materials*, 2001, 13(5): 1506-1511.
- <sup>22</sup>Gowd E B, Shibayama N, Tashiro K. Structural changes in thermally induced phase transitions of uniaxially oriented  $\delta_e$  form of syndiotactic polystyrene investigated by temperature-dependent measurements of X-ray fiber diagrams and polarized infrared spectra. *Macromolecules*, 2006, 39(24): 8412-8418.
- <sup>23</sup>Rizzo P, D'Aniello C, De Girolamo Del Mauro A, et al. Thermal transitions of  $\epsilon$  crystalline phases of syndiotactic polystyrene. *Macromolecules*, 2007, 40(26): 9470-9474.
- <sup>24</sup>Petraccone V, Ruiz de Ballesteros O, Tarallo O, et al. Nanoporous polymer crystals with cavities and channels. *Chemistry of Materials*, 2008, 20(11): 3663-3668.
- <sup>25</sup>Tarallo O, Schiavone M M, Petraccone V, et al. Channel clathrate of syndiotactic polystyrene with p-nitroaniline. *Macromolecules*, 2010, 43(3): 1455-1466.
- <sup>26</sup>Guerra G, Vitagliano V M, De Rosa C, et al. Polymorphism in melt crystallized syndiotactic polystyrene samples. *Macromolecules*, 1990, 23(5): 1539-1544.
- <sup>27</sup>Tamai Y, Fukuda M. Nanoscale molecular cavity in crystalline polymer membranes studied by molecular dynamics simulation. *Polymer*, 2003, 44: 3279-3289.
- <sup>28</sup>Milano G, Guerra G, Mueller-Plathe F. Anisotropic diffusion of small penetrants in the  $\delta$  crystalline phase of syndiotactic polystyrene: A molecular dynamics simulation study. *Chemistry of Materials*, 2002, 14(7): 2977-2982.
- <sup>29</sup>Tamai Y, Fukuda M. Fast one-dimensional gas transport in molecular capillary embedded in polymer crystal. *Chemical Physics Letters*, 2003, 371(1): 217-222.
- <sup>30</sup>Tamai Y, Fukuda M. Reorientational dynamics of aromatic molecules clathrated in  $\delta$  form of crystalline syndiotactic polystyrene. *Chemical Physics Letters*, 2003, 371(1): 620-625.
- <sup>31</sup>Tamai Y, Tsujita Y, Fukuda M. Reorientational relaxation of aromatic molecules in molecular cavity of crystalline syndiotactic polystyrene studied by molecular dynamics simulation. *Chemical Physics Letters*, 2005, 739(1): 33-40.
- <sup>32</sup>Figuroa-Gerstenmaier S, Daniel C, Milano G, et al. Storage of hydrogen as a guest of a nanoporous polymeric crystalline phase. *Physical Chemistry Chemical Physics*, 2010, 12(1): 5369-5374.
- <sup>33</sup>Figuroa-Gerstenmaier S, Daniel C, Milano G, et al. Hydrogen adsorption by  $\delta$  and  $\epsilon$  crystalline phases of syndiotactic polystyrene aerogels. *Macromolecules*, 2010, 43(20): 8594-8601.
- <sup>34</sup>Sanguigno L, Cosentino F, Larobina D, et al. Molecular simulation of carbon dioxide sorption in nanoporous crystalline phase of syndiotactic polystyrene. *Soft Materials*, 2011, 9(2-3): 169-182.
- <sup>35</sup>Yamamoto T. Molecular dynamics of crystallization in a helical polymer isotactic polypropylene from the oriented amorphous state. *Macromolecules*, 2014, 47: 3192-3202.
- <sup>36</sup>Strobl G. The physics of polymers: Concepts for Understanding Their Structures and Behavior, 3rd ed. Springer: Berlin, 2007.
- <sup>37</sup>Mueller-Plathe F. Coarse-graining in polymer simulation: from the atomistic to the mesoscopic scale and back. *ChemPhysChem*, 2002, 3(9): 754-769.
- <sup>38</sup>Voth G A. Coarse-graining of condensed phase and biomolecular systems. CRC press, 2008.
- <sup>39</sup>Peter C, Kremer K. Multiscale simulation of soft matter systems. *Faraday discussions*, 2010, 144: 9-24.

- <sup>40</sup>Milano G, Mueller-Plathe F. Mapping atomistic simulations to mesoscopic models: a systematic coarse-graining procedure for vinyl polymer chains. *The Journal of Physical Chemistry B*, 2005, 109(39): 18609-18619.
- <sup>41</sup>Spyriouni T, Tzoumanekas C, Theodorou D, et al. Coarse-grained and reverse-mapped united-atom simulations of long-chain atactic polystyrene melts: structure, thermodynamic properties, chain conformation, and entanglements. *Macromolecules*, 2007, 40(10): 3876-3885.
- <sup>42</sup>Qian H, Carbone P, Chen X, et al. Temperature-transferable coarse-grained potentials for ethylbenzene, polystyrene, and their mixtures. *Macromolecules*, 2008, 41(24): 9919-9929.
- <sup>43</sup>Sun Q, Faller R. Crossover from unentangled to entangled dynamics in a systematically coarse-grained polystyrene melt. *Macromolecules*, 2006, 39(2): 812-820.
- <sup>44</sup>Harmandaris V A, Adhikari N P, van der Vegt N F A, et al. Hierarchical modeling of polystyrene: from atomistic to coarse-grained simulations. *Macromolecules*, 2006, 39(19): 6708-6719.
- <sup>45</sup>Harmandaris V A, Reith D, van der Vegt N F A, et al. Comparison between coarse-graining models for polymer systems: two mapping schemes for polystyrene. *Macromolecular Chemistry and Physics*, 2007, 208: 2109-2120.
- <sup>46</sup>Fritz D, Harmandaris V A, Kremer K, et al. Coarse-grained polymer melts based on isolated atomistic chains: simulation of polystyrene of different tacticities. *Macromolecules*, 2009, 42(19): 7579-7588.
- <sup>47</sup>Brini E, Marcon V, van der Vegt N F A. Conditional reversible work method for molecular coarse graining applications. *Physical Chemistry Chemical Physics*, 2011, 13(1): 10468-10474.
- <sup>48</sup>Diechmann G, van der Vegt N F A. Conditional reversible work coarse-graining models of molecular liquids with coulomb electrostatics – A proof of concept study on weakly polar organic molecules. *The Journal of Chemical Theory and Computation*, 2017, 13: 6158-6166.
- <sup>49</sup>Mueller-Plathe F. Local structure and dynamics in solvent-swollen polymers. *Macromolecules*, 1996, 29(13): 4782-4791.
- <sup>50</sup>Hess B, Bekker H, Berendsen H J C, et al. LINCS: A Linear Constraint Solver for Molecular Simulations. *The Journal of Computational Chemistry*, 1997, 18(12): 1463-1472.
- <sup>51</sup>Sugita Y, Okamoto Y. Replica-exchange molecular dynamics method for protein folding. *Chemical Physics Letters*, 1999, 314(1): 141-151.
- <sup>52</sup>Hess B, Kutzner C, van der Spoel D, et al. GROMACS 4: Algorithms for highly efficient, load-balanced, and scalable molecular simulation. *The Journal of Chemical Theory and Computation*, 2008, 4(3): 435-447.
- <sup>53</sup>Bussi G, Donadio D, Parrinello M. Canonical sampling through velocity rescaling. *The Journal of Chemical Physics*, 2007, 126(1): 014101.
- <sup>54</sup>Berendsen H J C, Postma J P M, van Gunsteren W F, et al. Molecular dynamics with coupling to an external bath. *The Journal of Chemical Physics*, 1984, 81(8): 3684-3690.
- <sup>55</sup>Liu C, Muthukumar M. Langevin dynamics simulations of early-stage polymer nucleation and crystallization. *The Journal of Chemical Physics*, 1998, 109(6): 2536-2542.
- <sup>56</sup>Woo E M, Sun Y S, Yang C P. Polymorphism, thermal behavior, and crystal stability in syndiotactic polystyrene vs. its miscible blends. *Progress in Polymer Science*, 2001, 26: 945-983.